SANDIA REPORT

SAND2014-17469
Unlimited Release
Printed August 2014

A 3D Orthotropic Strain-Rate Dependent Elastic Damage Material Model

Shawn A. English

Prepared by
Sandia National Laboratories
Albuquerque, New Mexico 87185 and Livermore, California 94550

Sandia National Laboratories is a multi-program laboratory managed and operated by Sandia Corporation, a wholly owned subsidiary of Lockheed Martin Corporation, for the U.S. Department of Energy's National Nuclear Security Administration under contract DE-AC04-94AL85000.

Issued by Sandia National Laboratories, operated for the United States Department of Energy by Sandia Corporation.

Available to DOE and DOE contractors from
U.S. Department of Energy
Office of Scientific and Technical Information
P.O. Box 62
Oak Ridge, TN 37831

Telephone: (865) 576-8401
Facsimile: (865) 576-5728
E-Mail: reports@adonis.osti.gov
Online ordering: http://www.osti.gov/bridge

Available to the public from
U.S. Department of Commerce
National Technical Information Service
5285 Port Royal Rd.
Springfield, VA 22161

Telephone: (800) 553-6847
Facsimile: (703) 605-6900
E-Mail: orders@ntis.fedworld.gov
Online order: http://www.ntis.gov/help/ordermethods.asp?loc=7-4-0#online

SAND2014-17469
Unlimited Release
Printed August 2014

A 3D Orthotropic Elastic Damage and Failure Material Model

Shawn A. English
Multi-physics Modeling and Simulation
Sandia National Laboratories
P.O. Box 969
Livermore, CA 94551-0969

Abstract

A three dimensional orthotropic elastic constitutive model with continuum damage and cohesive based fracture is implemented for a general polymer matrix composite lamina. The formulation assumes the possibility of distributed (continuum) damage followed by localized damage. The current damage activation functions are simply partially interactive quadratic strain criteria. However, the code structure allows for changes in the functions without extraordinary effort. The material model formulation, implementation, characterization and use cases are presented.

CONTENTS

FIGURES

TABLES

1. MODEL FORMULATION

The material model outlined in this report follows closely to ones presented [1-4], with some notable differences. First, for simplicity the model assumes a quadratic summation of the strain to failure ratios for all damage activation functions. This is a simplification and can have some adverse effects in combined shear compression loading. However, changes in the activation functions would require experimental justification. For future iterations, the code allows for moderately simple changes in this regards. Second, damage evolution can be distributed, commonly associated with matrix damage, and/or localized, commonly associated with fiber failure. While the formulation for these damage mechanisms is similar, many distinctions exist as will be described below. Third, while hardening can be adjusted from linear with a damage exponent on the evolution variable, the softening behavior is assumed linear.

1.1. Damage

Elastic damage is assumed the only source of stiffness loss. Damage variables are introduced for each normal and shear direction. The corresponding compliance tensor takes on the following form [1]:

$$\mathbf{S} = \begin{bmatrix} \frac{1}{E_{11}(1-d_{11})} & \frac{-v_{21}}{E_{22}} & \frac{-v_{31}}{E_{33}} & 0 & 0 & 0 \\ \frac{-v_{12}}{E_{11}} & \frac{1}{E_{22}(1-d_{22})} & \frac{-v_{32}}{E_{33}} & 0 & 0 & 0 \\ \frac{-v_{13}}{E_{11}} & \frac{-v_{23}}{E_{22}} & \frac{1}{E_{33}(1-d_{33})} & 0 & 0 & 0 \\ 0 & 0 & 0 & \frac{1}{2G_{12}(1-d_{12})} & 0 & 0 \\ 0 & 0 & 0 & 0 & \frac{1}{2G_{13}(1-d_{13})} & 0 \\ 0 & 0 & 0 & 0 & 0 & \frac{1}{2G_{23}(1-d_{23})} \end{bmatrix} \quad (1)$$

where the active damage variable is function of the fiber and matrix damage variables as

$$d_{ij} = 1 - \left(1 - d_{ijm}\right)\left(1 - d_{ijf}\right) \quad (2)$$

The damaged (actual) stresses and strains are

$$\sigma_{ij} = C_{ijkl}\varepsilon_{kl} \quad (3)$$

$$\varepsilon_{ij} = S_{ijkl}\sigma_{kl} \quad (4)$$

where

$$C_{ijkl} = S_{ijkl}^{-1} \quad (5)$$

Since the compliance tensor becomes singular at $d = 1$, the stiffness tensor is written in closed form where the limit of stiffness as $d \rightarrow 1$ exists.

1.2. Initiation and Failure

A quadratic strain criterion is used for damage initiation and failure. The damage activation threshold is evaluated for tension and compression, matrix and fiber modes and for each of the primary material planes [2-4]. The damage activation function for the matrix mode in the 11 plane is given for tension and compression as function of the uniaxial (X) and shear (S) strengths and the elastic constants as

Tension:
$$\varphi_{11+}^{m} = \sqrt{\left(\frac{E_{11}\langle\varepsilon_{11}\rangle}{X_{11+}^{m}}\right)^2 + \left(\frac{G_{12}\gamma_{12}}{S_{12}^{m}}\right)^2 + \left(\frac{G_{13}\gamma_{13}}{S_{13}^{m}}\right)^2} \tag{6}$$

Compression:
$$\varphi_{11-}^{m} = \sqrt{\left(\frac{E_{11}\langle-\varepsilon_{11}\rangle}{X_{11-}^{m}}\right)^2 + \left(\frac{G_{12}\gamma_{12}}{S_{12}^{m}}\right)^2 + \left(\frac{G_{13}\gamma_{13}}{S_{13}^{m}}\right)^2} \tag{7}$$

where $\langle\ \rangle$ are the Macaulay brackets, defined as

$$\langle x\rangle = \begin{cases} 0, & x < 0 \\ x, & x \geq 0 \end{cases} \tag{8}$$

The user provides only damage initiation/failure stresses (X^f). For failure in the fiber mode the stress used in the damage activation function must be the effective stress. For strain equivalency, the effective strength in the 11 direction is simply

$$\bar{X}^f = E_{11}\varepsilon_{11}^f \tag{9}$$

where ε_{11}^f is the strain to failure found by solving strain during matrix damage curve at the fiber strength. Therefore, the damage activation function for the fiber mode in the 11 plane is given for tension and compression as

Tension:
$$\varphi_{11+}^{f} = \sqrt{\left(\frac{E_{11}\langle\varepsilon_{11}\rangle}{\bar{X}_{11+}^{f}}\right)^2 + \left(\frac{G_{12}\gamma_{12}}{\bar{S}_{12}^{f}}\right)^2 + \left(\frac{G_{13}\gamma_{13}}{\bar{S}_{13}^{f}}\right)^2} \tag{10}$$

Compression:
$$\varphi_{11-}^{f} = \sqrt{\left(\frac{E_{11}\langle-\varepsilon_{11}\rangle}{\bar{X}_{11-}^{f}}\right)^2 + \left(\frac{G_{12}\gamma_{12}}{\bar{S}_{12}^{f}}\right)^2 + \left(\frac{G_{13}\gamma_{13}}{\bar{S}_{13}^{f}}\right)^2} \tag{11}$$

1.3. Evolution Equations

The evolution of internal state variables resembles those in Maimí et al. [2, 3]. Differing from Miami's formulation, the damage evolution equations are different only for in-plane and out of plane for woven composites. For in-plane tensile and shear loading of a woven composite, damage evolution and "hardening" precede failure softening.

Begin with the consistency equation for each failure mechanism. For positive gradient of the loading function ($\dot{\phi}_i$) the consistency equation must be satisfied:

$$\dot{F}_i = \dot{\phi}_i - \dot{r}_i = 0 \tag{12}$$

where F_i and r_i are the damage activation function and damage threshold for mode i respectively. For damage evolution the Kuhn-Tucker conditions must be met

$$\dot{r}_i \geq 0 \ ; \qquad F_i \leq 0 \ ; \qquad F_i \dot{r}_i = 0 \tag{13}$$

Miami assumes the longitudinal and transverse damage evolutions are not coupled. This is debatable and would require experimental verification. This is simply done by examining the transverse strains and thus Poisson effect in a longitudinal loaded specimen with damage. For now this assumption will be incorporated for simplicity.

The damage evolution occurs in the direction normal to the damage surface [4], or

$$\frac{\partial r}{\partial \varepsilon} \dot{\varepsilon} > 0 \tag{14}$$

To satisfying this equation, the damage evolution for a single mode is assumed to have the following form

$$\dot{d} = \gamma \dot{r} \tag{15}$$

The desired damage evolution can be achieved by choosing the damage growth function as

$$\gamma = C_0 n r^{n-1} \tag{16}$$

Then the evolution of damage is simply

$$\dot{d} = C_0 n r^{n-1} \dot{r} \tag{17}$$

Integrating and applying the boundary conditions, the damage variables are given as

$$d = C_0 (r^n - 1) \tag{18}$$

Forcing linear hardening/softening when the damage exponent is 1 (n = 1), the above equation can be given as

$$d = \left(\frac{K}{E} - 1 \right) (r^n - 1) \tag{19}$$

where K is the damage modulus for linear hardening/softening and E is the elastic modulus. Fiber mode damage is assumed to linearly soften. Also, if matrix damage precedes fiber

damage, the elastic modulus is updated with the final matrix damage variable. For simplicity in energy calculations matrix damage is assumed complete when the damage variable reaches the monotonic uniaxial maximum achieved at first fiber failure.

1.3.1. Matrix Modes

Matrix damage evolution under tensile loading does not affect the compressive domain; conversely, matrix damage evolution under compressive loading does produce a tensile effect. The following equations provide the relationship

$$\begin{aligned} &\text{Tensile loading:} && \dot{r}_{im+} = \dot{\phi}_{im+} \text{ and } \dot{r}_{im-} = 0 \\ &\text{Compressive loading:} && \dot{r}_{im-} = \dot{\phi}_{im-} \text{ and } \dot{r}_{im-} = \begin{cases} \dot{\phi}_{im-} & \text{if } \dot{r}_{im+} \le \dot{r}_{im-} \\ 0 & \text{if } \dot{r}_{im+} > \dot{r}_{im-} \end{cases} \end{aligned} \tag{20}$$

Integrating these equations for time s = 0 to t, produces

$$r_{im+} = \max\left\{1, \max_{s=0,t}\{\phi^s_{im-}\}, \max_{s=0,t}\{\phi^s_{im+}\}\right\} \tag{21}$$

$$r_{im-} = \max\left\{1, \max_{s=0,t}\{\phi^s_{im-}\}\right\} \tag{22}$$

where i = 1, 2 or 3.

1.3.2. Fiber Modes

Fiber breaks under tensile loading can affect the compressive damage threshold. This evolution of compressive damage under tensile loading is proportional to the tensile damage by the coupling factor $A_{i\pm}$. The effective compressive fiber damage is then

$$d^{Eff}_{if-} = 1 - \left(1 - A_{i\pm} d_{if+}\right)\left(1 - d_{if-}\right) \tag{23}$$

where d_{if+} and d_{if-} are damages caused by tensile and compressive stresses respectively. Fiber breaks under compressive loading directly produces tensile damage. The following equations provide the relationship

$$\begin{aligned} &\text{Tensile loading:} && \dot{r}_{if+} = \dot{\phi}_{if+} \text{ and } \dot{r}_{if-} = 0 \\ &\text{Compressive loading:} && \dot{r}_{if-} = \dot{\phi}_{if-} \text{ and } \dot{r}_{if-} = \begin{cases} \dot{\phi}_{if-} & \text{if } \dot{r}_{if+} \le \dot{r}_{if-} \\ 0 & \text{if } \dot{r}_{if+} > \dot{r}_{if-} \end{cases} \end{aligned} \tag{24}$$

Integrating these equations for time s = 0 to t, produces

$$r_{if+} = \max\left\{1, \max_{s=0,t}\{\phi^s_{if-}\}, \max_{s=0,t}\{\phi^s_{if+}\}\right\} \tag{25}$$

$$r_{if-} = \max\left\{1, \max_{s=0,t}\{\phi^{s}_{if-}\}\right\} \quad (26)$$

The result is 12 damage evolution variables, 4 for each plane of damage (tension and compression for both matrix and fiber modes).

1.4. Loading Scenarios

Matrix mode damage evolution is limited to the fiber mode failure threshold. However, fiber mode damage is possible prior to matrix mode failure when fiber breaks occur in plane from a different component of strain. For example: fiber breaks under uniaxial tension and may not cause matrix damage, resulting in fiber breaks effecting subsequent shear loading. This and other important loading scenarios are shown below.

1.4.1. Tension then Compression

Under tensile stress the model predicts matrix damage ("hardening") followed by fiber breaks (softening). When the load is reversed, the matrix damage strain threshold is unaffected by the amount of fiber damage accumulated under tension and does not accumulate compressive stiffness loss due to tensile matrix damage. However, the fiber failure threshold is reduced due to tensile fiber breaks. The amount of tensile to compression fiber coupling is controlled by the coefficient $A_{\pm}$ from Equation (23). This type of coupling is assumed because tensile stresses generate crack planes normal to the loading direction, which may only partially affect the compressive response. Conversely, cracks generated by compressive loads will directly affect the tensile response.

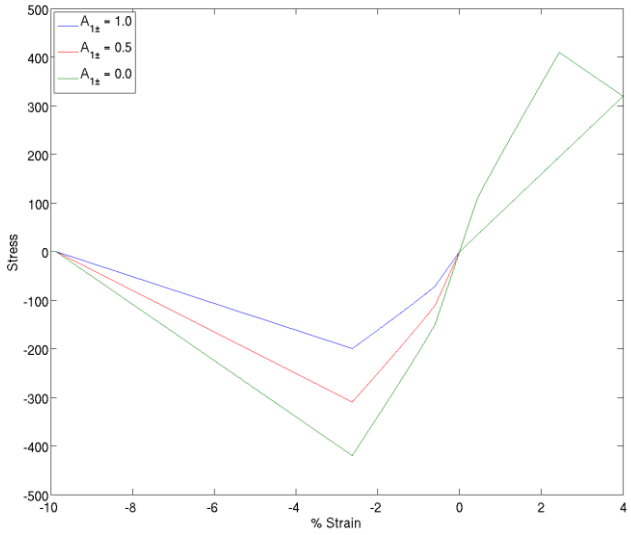

Figure 1: Axial stress-strain response with various compression-tension coupling

1.4.2. Compression then Tension

Under compressive stress the model predicts matrix damage (hardening) followed by fiber breaks (softening). Upon load reversal, no additional matrix damage occurs and the fiber damage accumulation continues. The matrix damage threshold can only increase if the current matrix damage is less than tensile matrix damage maximum.

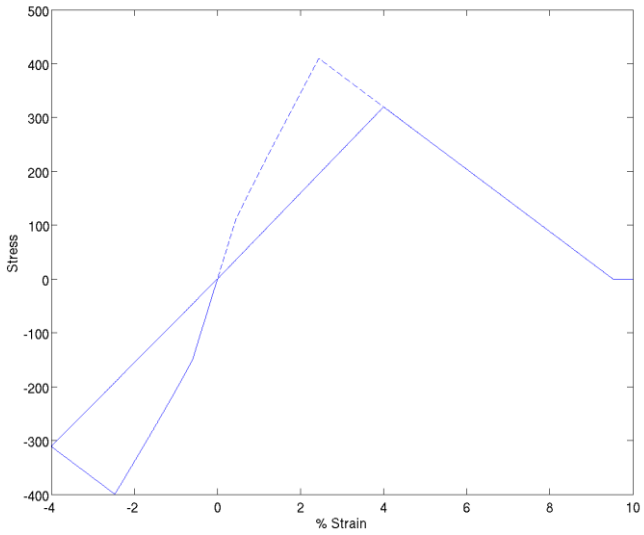

Figure 2: Axial stress-strain response for compression then tensile reversal

1.4.3. Tension then Shear without Fiber Failure

Figure 3 gives the stress versus time for longitudinal tension followed by in-plane shear. The shear response is set to continuously harden (shear stresses cannot cause fiber breaks). The matrix damage accumulation under tension affects the shear response.

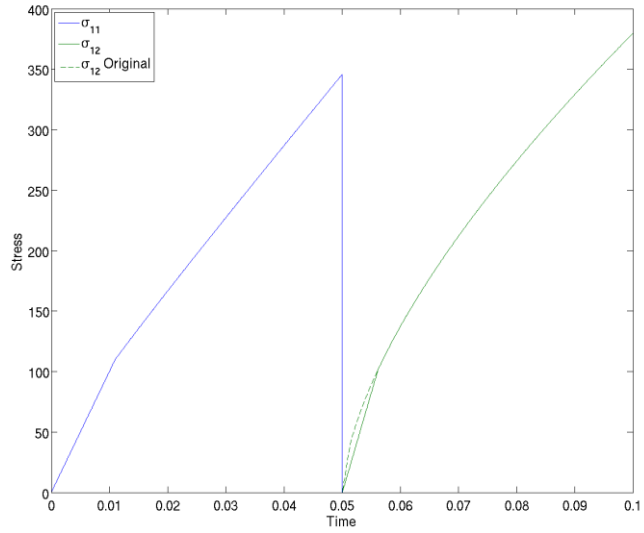

Figure 3: Axial and shear stress versus time with matrix damage only

1.4.4. Tension then Shear with Fiber Failure

Figure 4 gives the stress versus time for longitudinal tension and in-plane shear. The shear response is set to continuously harden (shear stresses cannot cause fiber breaks). While fiber breaks do not accumulate under shear, the response is affected if breaks occur from normal stresses. Both matrix damage and fiber breaks affect the shear response. Then matrix damage under shear continues.

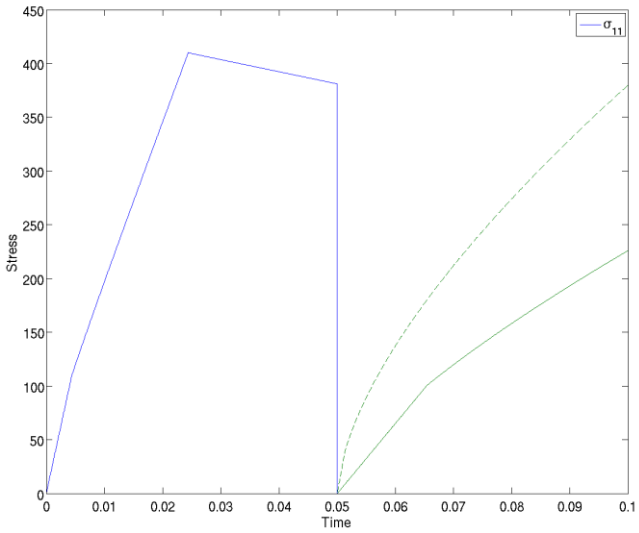

Figure 4: Axial and shear stress versus time with matrix and fiber damage

1.4.5. Shear then Tension with Fiber Failure

In this case, the shear response allows for fiber breaks. Similar to compression then tension, both matrix damage and fiber breaks accumulated under shear affect the tensile response.

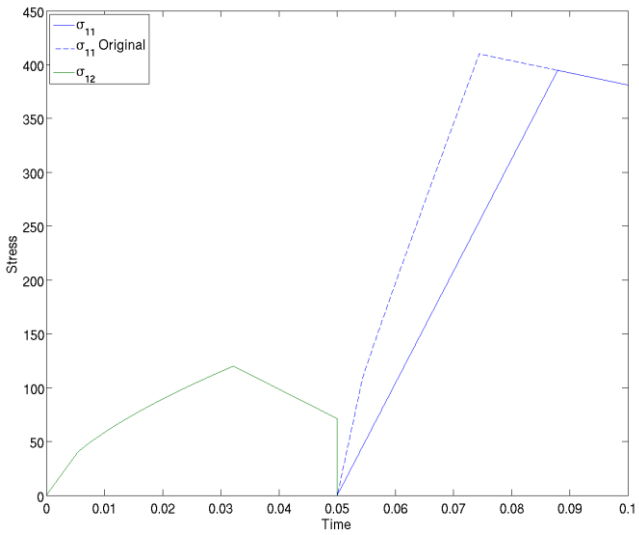

Figure 5: Shear and axial stress versus time with matrix and fiber damage

2. MATERIAL IDENTIFICATION

2.1. Failure Modes

Matrix mode failure is associated with matrix cracking and transverse yarn failure in woven lamina which is marked by non-linearity in the hardening region of the stress strain response. Therefore, matrix mode strength is the initial point of deviation from linear elasticity. For materials with response linear to peak stress, the user must specify the matrix mode strength to be greater than or equal to the fiber mode strength.

2.2. Fracture Energies

The user specified fracture energies are the total energy associated with material bifurcation for a given mode of failure. The current model formulation does not account for mixed mode coupling during fracture.

Crack band theory assumes that a band of continuously distributed parallel cracks [5] releases the same energy as a line crack. The opening stress to relative displacement (δ) relationship is therefore replaced with the presumed identical $\delta = \varepsilon l^*$, where, for our purposes, l^* is the characteristic length of the finite element and ε is the homogenized strain in the crack opening direction.

In three-dimensional finite element analysis, the crack growth direction is associated with the homogenized energy released during material failure. Therefore, the failure plane must be known a priori. For orthotropic materials, the failure plane is often one of the principal material planes. Therefore, best practice is to use cube hexagonal elements oriented in the material system, in which the characteristic length is simply the edge length associated with each integration point [2]. Where the crack direction is arbitrary in a plane, the characteristic length for a cube element is

$$l^* = \frac{\sqrt{A_{IP}}}{\cos\theta} \tag{27}$$

where θ is the angle between mesh and the crack direction and A_{IP} is the in-plane area of the element associated with each integration point. Also, the average can be used for an unknown crack as [2]

$$l^* = \frac{4}{\pi}\int_0^{\frac{\pi}{4}} l^* d\theta \ = 1.12\sqrt{A_{IP}} \tag{28}$$

For example, a 1x1x1 single integration point element assigned a material oriented +45 degrees about the out-of-plane axis would have a characteristic length equal to $\sqrt{2}$.

Each set of internal parameters associated with fracture are calculated independently for each mode of failure: monotonic tension/compression and pure shear. The initialization routine determines the softening slope of the stress strain response so the total dissipated fracture energy (area under σ-εl^* curve) is equal to the user specified fracture energy. A critical element size criterion is evaluated. The element size (characteristic length l^*) must satisfy:

$$l^* \leq \frac{G_f}{\int_0^{\varepsilon_f} \sigma \, d\varepsilon} \tag{29}$$

for all modes of failure, where ε_f is the strain to fiber mode failure. For example, a material with linear elastic to peak stress has a critical element criterion for axial tension of

$$l^* \leq \frac{2G_{I11}E_{11}}{X_{f11}^2} \tag{30}$$

where G_{I11} is the fracture energy associated with bifurcation under axial tension.

2.3. Damage Evolution

Damage evolution is user defined only for matrix mode failure. The evolution of fiber damage is controlled by internal parameters using the fracture energies and crack band theory. For each matrix failure mode (tension, compression, shear) the evolution equation is generally defined as

$$d = 1 - \frac{K_m}{E} + \left(\frac{K_m}{E} - 1\right)\frac{1}{r_m^n} \tag{31}$$

where K_m and n are the matrix mode damage modulus and exponent respectively. The damage exponent is intended to add flexibility in the material response. For shear damage, K_m is defined in terms of classical (engineering) shear strain γ. After the fiber mode strength is exceeded, the material is linearly softened. Note matrix mode damage is zero for $K_m = E$ or $n = 0$. Figure 6 shows the effects of n for an arbitrary shear response.

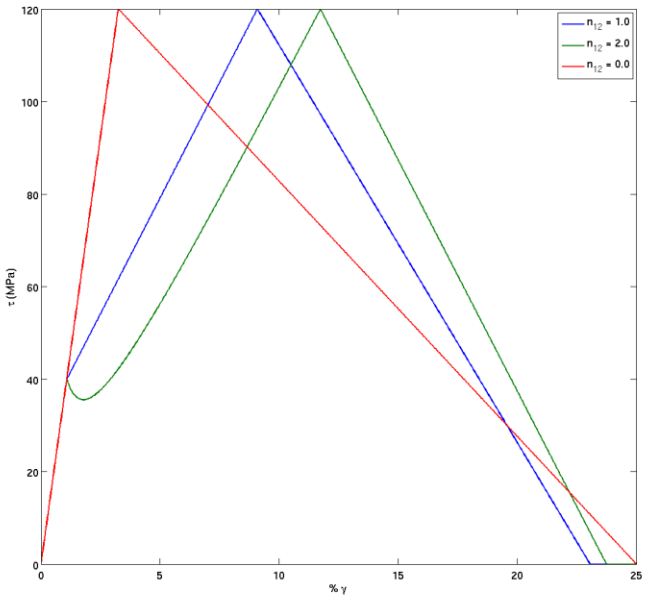

Figure 6: Shear stress-strain response with various damage exponents

2.4. Rate Dependency

Purely empirical strain rate dependence is included. Rate dependencies use the following relationship [6]:

$$A = \bar{A}\left(1 + m_r log \frac{\dot{\varepsilon}}{\dot{\varepsilon}_o}\right) \tag{32}$$

where A and $\bar{A}$ are the rate effected and reference material properties respectively, m_r is the rate coefficient and $\dot{\varepsilon}_o$ is the reference strain rate used to determine $\bar{A}$. An independent rate equation is utilized for each elastic stiffness, matrix mode strength and fiber mode strength. Rate is assumed to affect tension and compression equally.

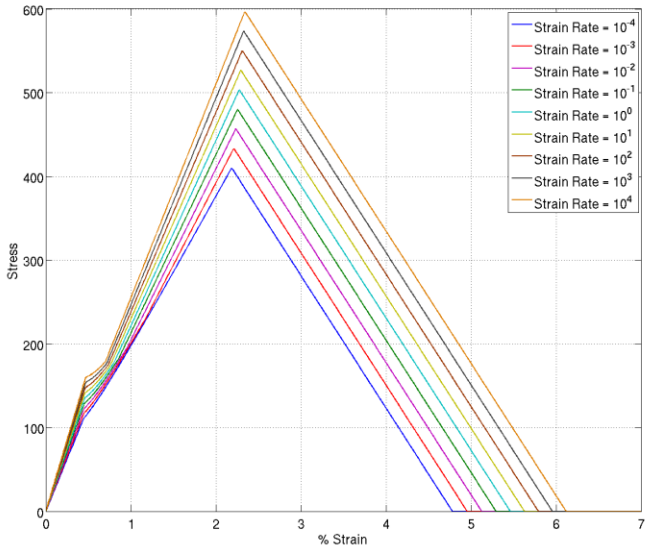

Figure 7: Stress-strain response at various strain rates

2.5. Control Fracture

The control fracture methodology in Sierra is implemented to ensure timestep independence in implicit analysis. Control fracture iteratively kills elements exhibiting the highest measure of failure then recalculates. Internally, the material model with the control fracture methodology utilizes failure flags to designate states of failure. For implicit analysis, the states are 0, 1, 2, 3, and 4 corresponding to not failed, exceeds failure criteria, chosen to fail, decaying and fully decayed respectively.

The material model provides the option to utilize the control fracture method in two different ways. The first (default) method utilizes control fracture for the first fiber mode failure detected then remains in the decaying region until all fiber modes are complete. The basis for this method is to allow elements to behave as if fibers are still attached in the direction transverse

to the crack. The second method reduces all stresses to zero when a single fiber mode has completed. This essentially kills the element i.e.

$$d_{ij}^f = max\left(d_{ij}^f\right) \quad \text{for} \quad d_{ij}^f > 0.0 \tag{33}$$

Upon complete failure ($max\left(d_{ij}\right) = 1.0$)) the failure flag is set to 4 (complete decay).

In order to demonstrate the effect of the control fracture method a simple notched plate under tension is simulated. Distributed (matrix) damage accumulates along the likely crack path and appears as a cloud. Conversely, the fiber failure is iteratively solved for each timestep using control fracture and, therefore, follows a single element thick crack path. Contour plots for this simulation are shown in Figure 8.

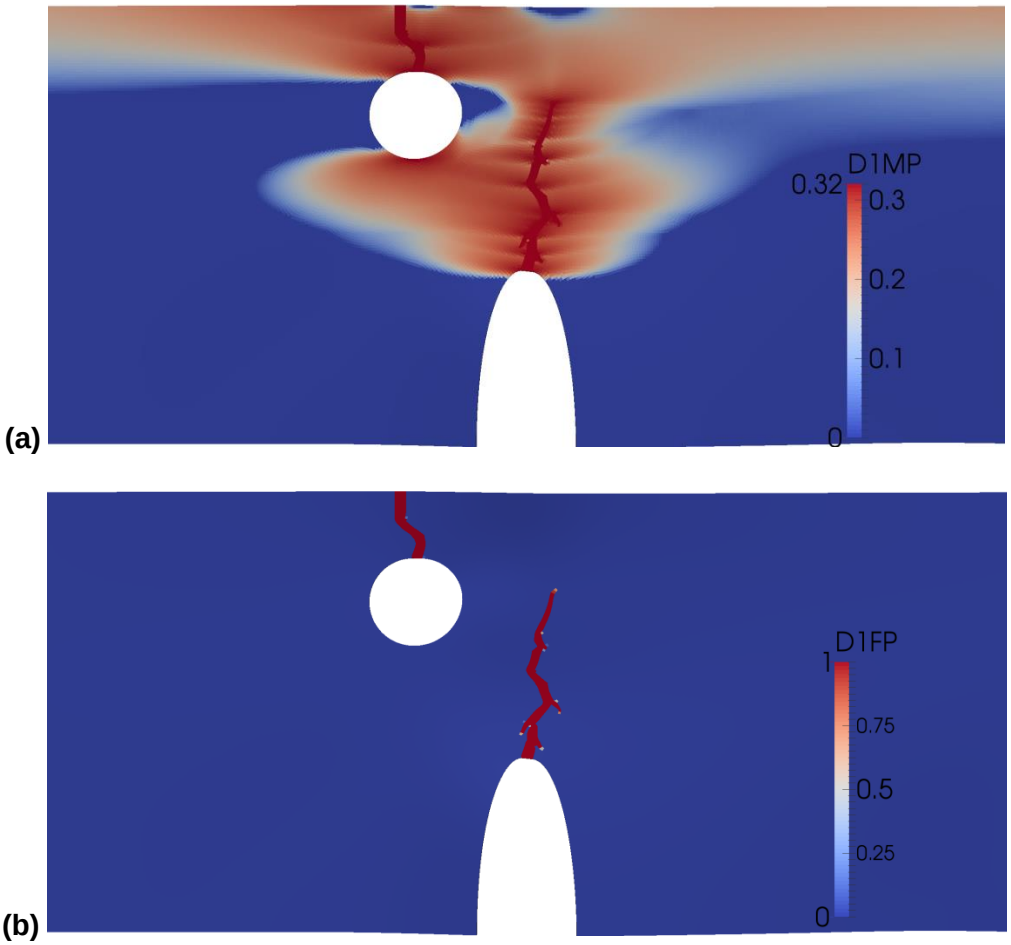

Figure 8: Tensile loaded notched plate with (a) matrix and (b) fiber damage

2.6. Element Death Considerations

While not necessary for small deformations, element death can be used in conjunction with this material model in order to simulate crack growth. If an element is determined dead, material

connectivity is ignored. For many orthotropic materials the crack plane is assumed one of the primary material directions. In this case, element death is optional. If the element is not killed upon directional failure, the stiffness remains in the intact directions.

While the crack flag is triggered under compressive stresses, limiting the damage with the maximum compressive damage parameter (< 1.0), results in an element that never fails. In this case a maximum compressive strain criterion is recommended for element death in order to prevent timestep and element quality issues.

The most robust death criteria that ensures proper energy dissipation and mesh quality is simply based on the components of damage, or $d_{ij} = 1.0$, where d_{ij} are defined in Equation (2) as the total active damages and the state variable vector name is DAMAGE.

3. EXAMPLE PROBLEMS

3.1. Ballistic Penetration

A high velocity penetration analysis is conducted with a four layer eight harness satin weave (8HS) carbon fiber reinforced polymer (CFRP) 50mm x 50mm unsupported plate. The impactor is a 4.5 mm diameter sphere traveling at 500 m/s. The material is a four layer carbon fiber laminate. The material properties are similar to those in the subsequent section, but are used for demonstrative purposed only. The change in average kinetic energy of the projectile is used as metric for mesh convergence.

While the material model allows for cohesive like out-of-plane failure, it is assumed delamination is the dominate failure mechanism. From various iterations of model types, cohesive zone elements with explicitly defined lamina to lamina contact are the best way to model interlaminar failure. More details on cohesive zone elements and contact are given in Appendix B. The laminas are modeled as individual blocks separated by the zero-volume element and initially collocated side sets or block surfaces are given a contact definition. This method does not rely on a penetration multiplier, which can cause convergence issues and tends to allow penetration after shear mode failure. Figure 9a shows the results when a penetration stiffness multiplier is used and Figure 9b shows the result of using contact between layers.

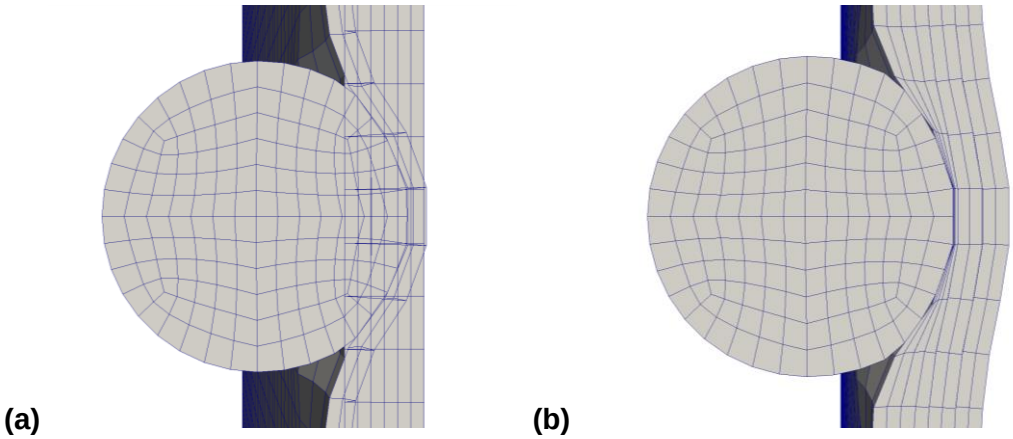

Figure 9: Penetration simulations with and without interlaminar contact

In order to achieve a mesh convergent solution, the characteristic length of the failure model is modified based on estimated fracture area associated with mesh size. Figure 10 shows the total kinetic energy of the penetrator versus simulation time for four mesh sizes each with an edge length reduction factor of 2. While the time history is slightly different for finest mesh, the final change of kinetic energy appears mesh convergent. Note, the coarsest mesh demonstrated a punch failure while the three finer meshes showed a qualitatively similar petal type failure (see Figure 11).

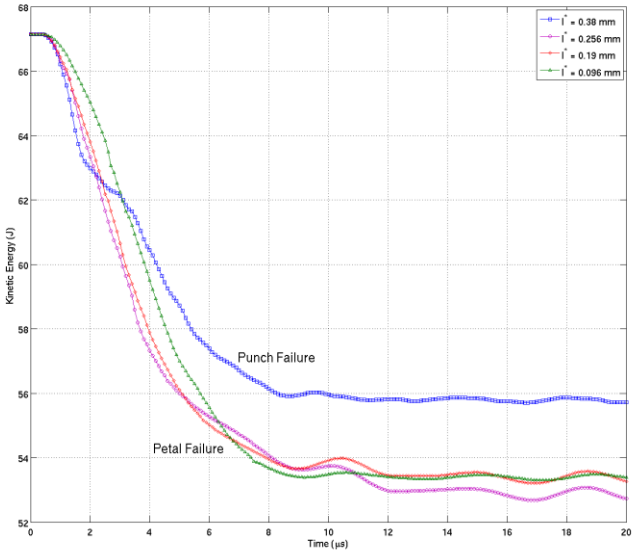

Figure 10: Total kinetic energy of the penetrator versus simulation time for various mesh sizes (characteristic lengths)

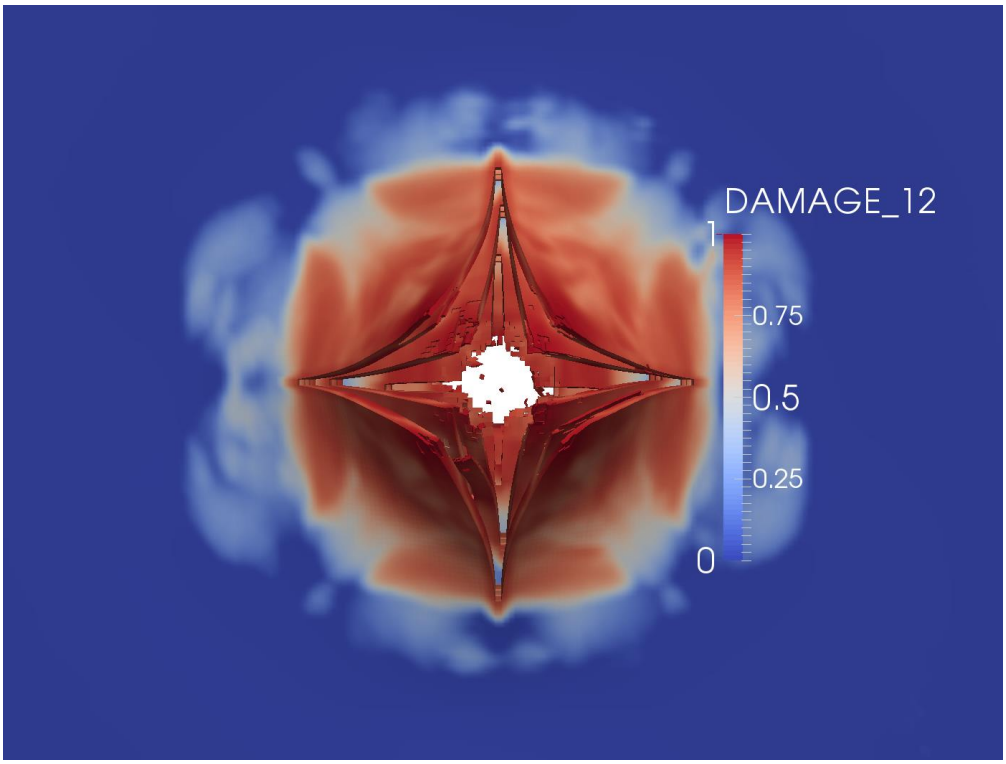

Figure 11: Petal type penetration failure with in plane damage, shown without penetrator

3.2. Low-Velocity Impact

This validation effort is documented in an accompanying SAND report. Model description and pertinent results are presented here. The dimensions for the test specimen are given in Table 1. For the textile architecture used in this study, one ply is denoted as (0/90) representing the warp and fill directions in the 0° and 90° directions, respectively. Therefore, the laminates used in this investigation were composed of 12 plies of textile material with the warp direction oriented along the specimen's length. The indenter has a 19 mm diameter cylindrical tup with a mass of 5.42 kg. The impact energy for this demonstration is approximately 50J.

Table 1: Typical dimensions for impact specimens

Width (mm)	Length (mm)	Thickness (mm)	Stack Sequence
102	*155*	*4.49*	$[(0/90)_6]_s$

The CFRP material properties are measured, calibrated to experiments, calculated with micromechanics, obtained from literature or estimated using engineering judgment. The values used for this example are shown in Table 2. Standard deviations are given in parentheses and bounds of uniform distributions are shown as ±.

Table 2: CFRP material properties

Identification	Values	Identification	Values
E_{11} *(GPa)*	*63.9 (2.4)*	F_{1T} *(MPa)*	*769 (37)*
E_{22} *(GPa)*	*62.7 (3.8)*	F_{1C} *(MPa)*	*-816 (69)*
E_{33} *(GPa)*	*8.19 ± 0.40*	F_{2T} *(MPa)*	*823 (26)*
v_{12}	*0.048 (0.018)*	F_{2C} *(MPa)*	*-816 (69)*
v_{23}	*0.399 ± 0.018*	F_{3T} *(MPa)*	*56.2 ± 13*
v_{13}	*0.400 ± 0.017*	F_{3C} *(MPa)*	*-56.2 ± 13*
G_{12} *(GPa)*	*3.44 (0.058)*	S_{12M} *(MPa)*	*48.4 (0.84)*
G_{23} *(GPa)*	*3.27 ± 0.27*	S_{12F} *(MPa)*	*77.3 (1.1)*
G_{13} *(GPa)*	*3.25 ± 0.26*	S_{23M} *(MPa)*	*32.4 ± 7.4*
G_{I11}	*80 ± 20*	S_{23F} *(MPa)*	*65.5 ± 12*
G_{I22}	*80 ± 20*	S_{13M} *(MPa)*	*32.4 ± 7.4*
G_{I33}	*2.6 ± 2.5*	S_{13F} *(MPa)*	*65.5 ± 12*
G_{II12}	*12 ± 1.2*	K_{12m} *(MPa)*	*152 (10.1)*
G_{II23}	*10 ± 1.0*	K_{23m} *(MPa)*	*152 ± 15.2*
G_{II13}	*10 ± 1.0*	K_{13m} *(MPa)*	*152 ± 15.2*

The finite element mesh is shown in Figure 12. While many simulations where conducted for validation assessment, a single run is shown for demonstrative purposes. The load time history is shown in Figure 13. The model and experimental results are smoothed and filtered respectively to remove high frequency noise. The out-of-plane shear damage and delamination contours are shown for the warp cross-section along with a comparison computed tomography (CT) image from the experiments in Figure 14.

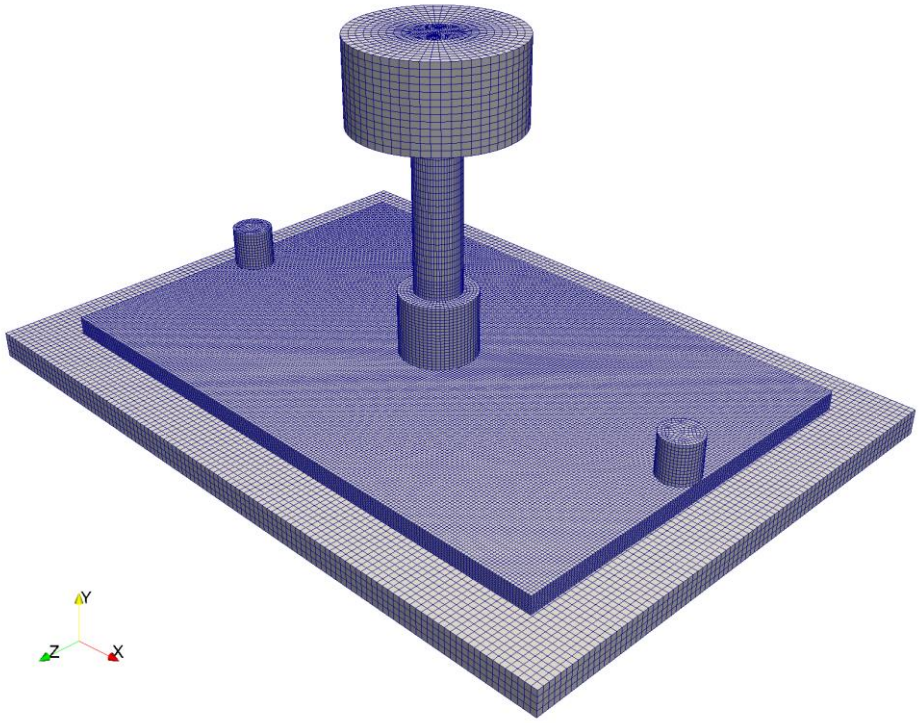

Figure 12: Full mesh of simulated low velocity impact experiment (note: x-plane symmetry is utilized)

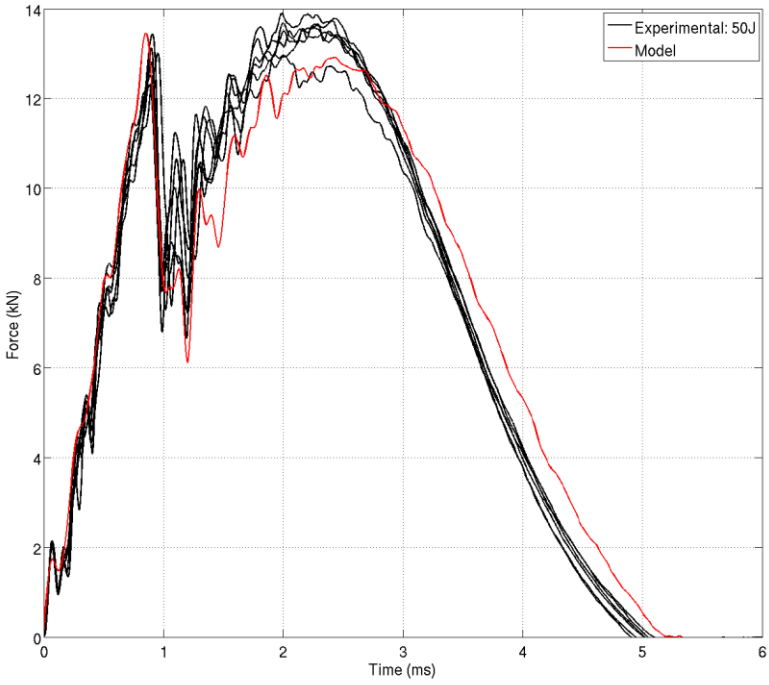

Figure 13: Force versus time from simulation and experiments

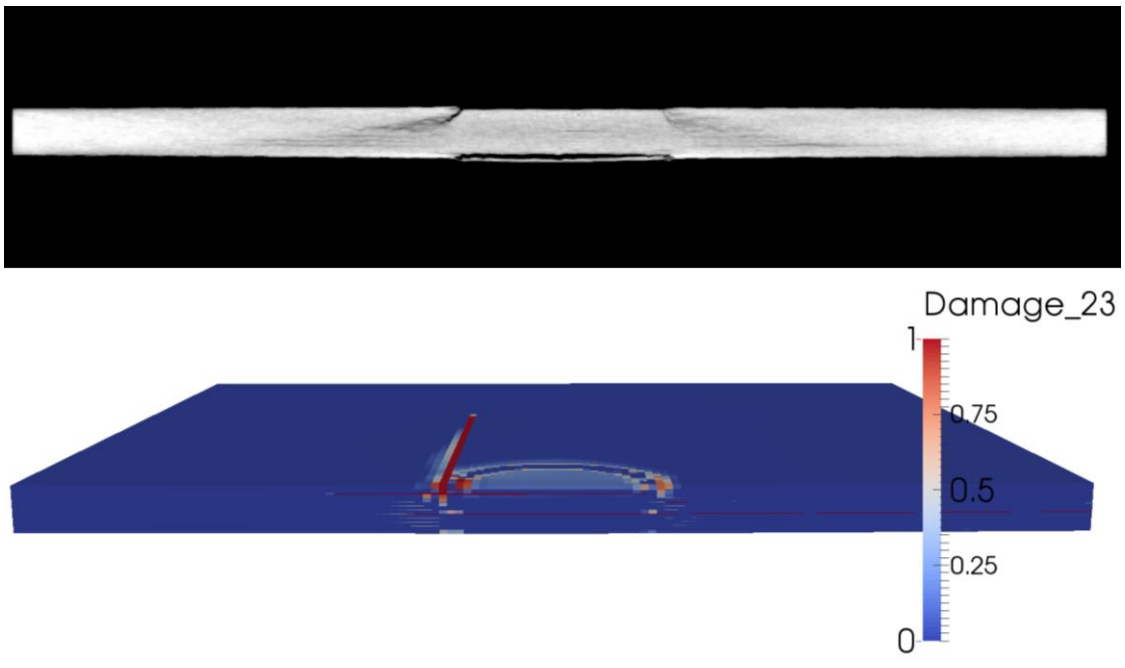

Figure 14: The post impact cross-section of (a) CT scanned specimen and (b) model prediction of out-of-plane damage and delamination. Note, the scan is taken from a material with slightly different matrix but otherwise identical

4. CONCLUSIONS

A general phenomenological orthotropic damage and failure material model has been detailed and user guidance, material characterization and examples are provided. The resulting constitutive model is relevant for many composite materials. In addition, the general framework and orthotropic orientation capabilities provide adaptability for future damage evolution/failure models.

5. REFERENCES

[1] A. Matzenmiller, J. Lubliner, and R. Taylor, "A constitutive model for anisotropic damage in fiber-composites," *Mech. of Mat.,* vol. 20, pp. 125-152, (1995).

[2] P. Maimí, P. Camanho, J. Mayugo, and C. Dávila, "A continuum damage model for composite laminates: Part II – Computational implementation and validation," *Mech. of Mat.,* vol. 39, pp. 909-919, (2007).

[3] P. Maimí, P. Camanho, J. Mayugo, and C. Dávila, "A continuum damage model for composite laminates: Part I – Constitutive model," *Mech. of Mat.,* vol. 39, pp. 897-908, (2007).

[4] *User's Manual for LS-Dyna MAT162 Unidirectional and Plain Weave Composite Progressive Failure Models*, Newark, DE: Center for Comp. Mat., 2011.

[5] Z. P. Bazant, and B. H. Oh, "Crack band theory for fracture of concrete," *Matériaux et Construction,* vol. 16, pp. 155-177, 1983.

[6] I. Daniel, B. Werner, and J. Fenner, "Strain-rate-dependent failure criteria for composites," *Comp. Sci. and Tech.,* vol. 71, pp. 357-364, 2011.

[7] K. W. Gan, S. R. Hallett, and M. R. Wisnom, "Measurement and modelling of interlaminar shear strength enhancement under moderate through-thickness compression," *Comp. Part A,* vol. 49, pp. 18-25, (2013).

[8] S. Li, M. Thouless, A. Waas, J. Schroeder, and P. Zavattieri, "Mixed-mode Cohesive-zone Models for Fracture of an Adhesively-bonded Polymer-matrix Composite," *Eng. Fract. Mech.,* vol. 73, pp. 64-78, (2006).

APPENDIX A: SIERRA MATERIAL MODEL SYNTAX

Elastic Orthotropic Continuous Damage Mechanics Material Model:

```
BEGIN MATERIAL <string>mat_name
   DENSITY = <real>density_value
   BIOTS COEFFICIENT = <real>biots_value
   BEGIN PARAMETERS FOR MODEL ELASTIC_ORTHOTROPIC_FAIL
        # General parameters (any two are required)
        YOUNGS MODULUS    = <real>youngs_modulus
        POISSONS RATIO    = <real>poissons_ratio
        SHEAR MODULUS     = <real>shear_modulus
        BULK MODULUS      = <real>bulk_modulus
        LAMBDA            = <real>lambda
        # Required parameters
        E11               = <real>e11
        E22               = <real>e22
        E33               = <real>e33
        NU12              = <real>nu12
        NU13              = <real>nu13
        NU23              = <real>nu23
        G12               = <real>g12
        G13               = <real>g13
        G23               = <real>g23
        # Normal thresholds
        TENSILE_MATRIX_STRENGTH_11     = <real>f1mp
        COMPRESSIVE_MATRIX_STRENGTH_11 = <real>f1mn
        TENSILE_FIBER_STRENGTH_11      = <real>f1fp
        COMPRESSIVE_FIBER_STRENGTH_11  = <real>f1fn
        TENSILE_MATRIX_STRENGTH_22     = <real>f2mp
        COMPRESSIVE_MATRIX_STRENGTH_22 = <real>f2mn
        TENSILE_FIBER_STRENGTH_22      = <real>f2fp
        COMPRESSIVE_FIBER_STRENGTH_22  = <real>f2fn
        TENSILE_MATRIX_STRENGTH_33     = <real>f3mp
        COMPRESSIVE_MATRIX_STRENGTH_33 = <real>f3mn
        TENSILE_FIBER_STRENGTH_33      = <real>f3fp
        COMPRESSIVE_FIBER_STRENGTH_33  = <real>f3fn
        # Shear thresholds
        SHEAR_MATRIX_STRENGTH_12       = <real>s12m
        SHEAR_FIBER_STRENGTH_12        = <real>s12f
        SHEAR_MATRIX_STRENGTH_23       = <real>s23m
        SHEAR_FIBER_STRENGTH_23        = <real>s23f
        SHEAR_MATRIX_STRENGTH_13       = <real>s13m
        SHEAR_FIBER_STRENGTH_13        = <real>s13f
        # Fracture parameters
        TENSILE_FRACTURE_ENERGY_11     = <real>gi1p
        COMPRESSIVE_FRACTURE_ENERGY_11 = <real>gi1n
```

```
TENSILE_FRACTURE_ENERGY_22     = <real>gi2p
COMPRESSIVE_FRACTURE_ENERGY_22 = <real>gi2n
TENSILE_FRACTURE_ENERGY_33     = <real>gi3p
COMPRESSIVE_FRACTURE_ENERGY_33 = <real>gi3n
SHEAR_FRACTURE_ENERGY_12       = <real>gii12
SHEAR_FRACTURE_ENERGY_23       = <real>gii23
SHEAR_FRACTURE_ENERGY_13       = <real>gii13
CHARACTERISTIC_LENGTH          = <real>l_star
#Damage evolution parameters
MAXIMUM_COMPRESSIVE_DAMAGE_11  = <real>dmax1n
MAXIMUM_COMPRESSIVE_DAMAGE_22  = <real>dmax2n
MAXIMUM_COMPRESSIVE_DAMAGE_33  = <real>dmax3n
COMPRESSION_COUPLING_FACTOR_11 = <real>a1pn
COMPRESSION_COUPLING_FACTOR_22 = <real>a2pn
COMPRESSION_COUPLING_FACTOR_33 = <real>a3pn
TENSILE_DAMAGE_MODULUS_11      = <real>k1p
COMPRESSIVE_DAMAGE_MODULUS_11  = <real>k1n
TENSILE_DAMAGE_MODULUS_22      = <real>k2p
COMPRESSIVE_DAMAGE_MODULUS_22  = <real>k2n
TENSILE_DAMAGE_MODULUS_33      = <real>k3p
COMPRESSIVE_DAMAGE_MODULUS_33  = <real>k3n
SHEAR_DAMAGE_MODULUS_12        = <real>k12
SHEAR_DAMAGE_MODULUS_23        = <real>k23
SHEAR_DAMAGE_MODULUS_13        = <real>k12
HARDENING_EXPONENT_11          = <real>n11
HARDENING_EXPONENT_22          = <real>n22
HARDENING_EXPONENT_33          = <real>n33
HARDENING_EXPONENT_12          = <real>n12
HARDENING_EXPONENT_23          = <real>n23
HARDENING_EXPONENT_13          = <real>n13
# Strain rate dependent parameters
REFERENCE_STRAIN_RATE          = <real>epsdot0
ELASTIC_RATE_COEFFICIENT_11    = <real>ce11
ELASTIC_RATE_COEFFICIENT_22    = <real>ce22
ELASTIC_RATE_COEFFICIENT_33    = <real>ce33
ELASTIC_RATE_COEFFICIENT_12    = <real>ce12
ELASTIC_RATE_COEFFICIENT_23    = <real>ce23
ELASTIC_RATE_COEFFICIENT_13    = <real>ce13
FIBER_STRENGTH_RATE_COEFFICIENT_11  = <real>cf11
FIBER_STRENGTH_RATE_COEFFICIENT_22  = <real>cf22
FIBER_STRENGTH_RATE_COEFFICIENT_33  = <real>cf33
FIBER_STRENGTH_RATE_COEFFICIENT_12  = <real>cf12
FIBER_STRENGTH_RATE_COEFFICIENT_23  = <real>cf23
FIBER_STRENGTH_RATE_COEFFICIENT_13  = <real>cf13
MATRIX_STRENGTH_RATE_COEFFICIENT_11 = <real>cm11
MATRIX_STRENGTH_RATE_COEFFICIENT_22 = <real>cm22
MATRIX_STRENGTH_RATE_COEFFICIENT_33 = <real>cm33
```

```
   MATRIX_STRENGTH_RATE_COEFFICIENT_12 = <real>cm12
   MATRIX_STRENGTH_RATE_COEFFICIENT_23 = <real>cm23
   MATRIX_STRENGTH_RATE_COEFFICIENT_13 = <real>cm13
   # Coefficient of thermal expansion functions
   THERMAL_STRAIN_11_FUNCTION = <string>cte11_function_name
   THERMAL_STRAIN_22_FUNCTION = <string>cte22_function_name
   THERMAL_STRAIN_33_FUNCTION = <string>cte33_function_name
   # Temperature dependent property functions
   E11_FUNCTION  = <string>e11_function_name
   E22_FUNCTION  = <string>e22_function_name
   E33_FUNCTION  = <string>e33_function_name
   NU12_FUNCTION = <string>nu12_function_name
   NU23_FUNCTION = <string>nu23_function_name
   NU13_FUNCTION = <string>nu13_function_name
   G12_FUNCTION  = <string>g12_function_name
   G23_FUNCTION  = <string>g23_function_name
   G13_FUNCTION  = <string>g13_function_name
   # Orientation
   ANGLE_1_ABSCISSA  = <real>angle_1_abscissa
   ANGLE_2_ABSCISSA  = <real>angle_2_abscissa
   ANGLE_3_ABSCISSA  = <real>angle_3_abscissa
   ROTATION_AXIS_1   = <real>rotation_axis_1
   ROTATION_AXIS_2   = <real>rotation_axis_2
   ROTATION_AXIS_3   = <real>rotation_axis_3
   ANGLE_1_FUNCTION  = <string>angle_1_function_name
   ANGLE_2_FUNCTION  = <string>angle_2_function_name
   ANGLE_3_FUNCTION  = <string>angle_3_function_name
   COORDINATE SYSTEM = <string>coordinate_system_name
END [PARAMETERS FOR MODEL ELASTIC_ORTHOTROPIC_FAIL]
```

APPENDIX B: COMPRESSION EFFECTED TRACTION SEPARATION LAW FOR COHESIVE ZONE MODELING

Cohesive elements do not behave well under out-of-plane compressive loads. A common practice is to apply an interpenetration stiffness. This practice often produces unrealistic results under high levels of compression, such as are found in penetration analysis. An alternative is to define contact between adjacent faces making up the cohesive element. The contact algorithm then calculates the necessary forces to prevent interpenetration. This method has an additional benefit of friction. Utilizing friction between faces essentially results in a simple compression dependent cohesive model similar to [7]. A simple mixed mode traction separation law detailed in [8] is used for delamination prediction. Therefore, for a constant normal stress (σ_n), the effective peak traction and toughness are simply

$$\tau^* = \tau + \mu\langle -\sigma_n \rangle \tag{34}$$

$$G_{II}^* = G_{II} + \mu\delta_{TC}\langle -\sigma_n \rangle \tag{35}$$

where μ is the frictional coefficient and δ_{TC} is the critical tangential separation. Since after element failure a frictional interface is assumed, the current model cannot differentiate surfaces enclosing a failed element, i.e. a single friction coefficient controls both CZ traction and frictional forces on the crack faces. The model form is known to be in error in this regard. In order to remedy this deficiency a novel approach is proposed.

While not utilized in any of the mentioned analysis, the following method for compression dependent traction separation is proposed. A nodal variable dependent coulomb friction law is used to define the interaction between parallel faces separated by a cohesive zone element. A user subroutine is used to calculate the instantaneous friction coefficient for a given compressive stress and tangential displacement. The variable inputs are the contact normal force (F_n) and a special monotonic tangential separation parameter (δ) added to the traction-separation material model.

$$\begin{array}{ll}
\delta \le \delta_1 & \begin{array}{c} \mu = 0.0 \\ \tau = K_1\delta \end{array} \\
\delta_1 < \delta \le \delta_{1f} & \begin{array}{c} \mu = (K_1 - K_2)(\delta - \delta_1)/\sigma_n \\ \tau = \tau_o + K_2(\delta - \delta_1) + \mu\sigma_n \end{array} \\
\delta_{1f} < \delta \le \delta_t & \begin{array}{c} \mu = \mu_f \\ \tau = \tau_o + K_2(\delta - \delta_1) + \mu\sigma_n \end{array} \\
\delta_t < \delta \le \delta_c & \begin{array}{c} \mu = \mu_f + K_2(\delta - \delta_t)/\sigma_n \\ \tau = \mu\sigma_n \end{array} \\
\delta > \delta_c & \begin{array}{c} \mu = \mu_c \\ \tau = \mu\sigma_n \end{array}
\end{array} \tag{36}$$

where $\sigma_n = -F_n/A_n$ and A_n is the area associated with the nodes in contact.

Figure 15 shows the effect of load angle for displacement control traction. Figure 16 provides the related effective toughness. Figure 17 shows the shape of the friction coefficient curve for nearly zero and a constant compressive stress. Similarly, Figure 18 shows the traction separation laws for these conditions.

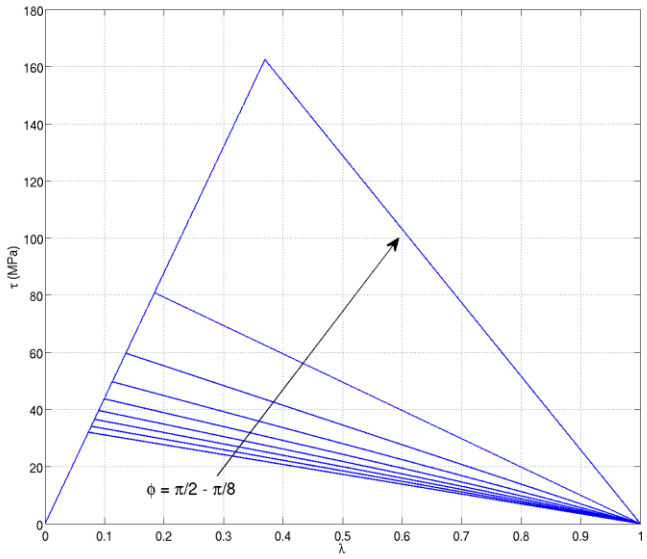

Figure 15: Traction separation laws for various load angles. The compressive stress is applied as $\sigma_n = \tau\cot(\phi)$

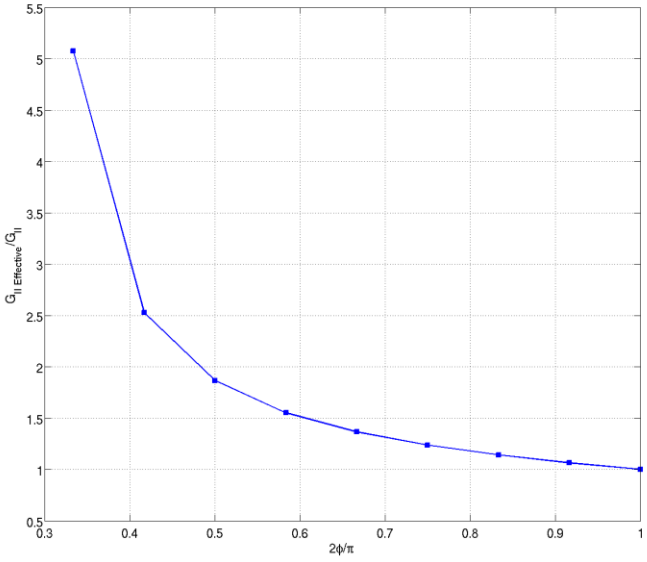

Figure 16: Effective energy release rate versus load angle ($\phi = \pi/2$ *is pure shear)*

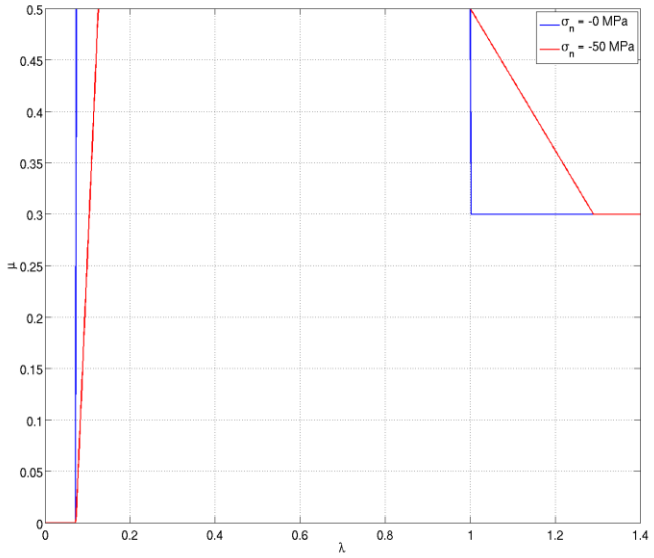

Figure 17: Example of the applied friction coefficient versus λ for constant compressive stresses. Negative zero refers to a negligibly small compressive force.

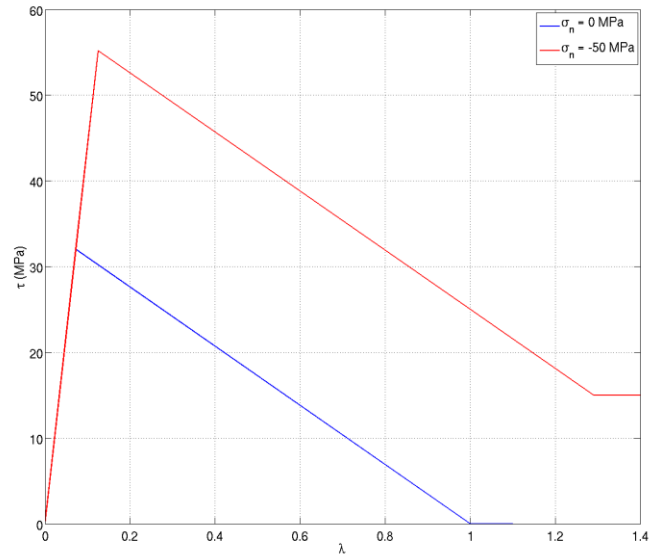

Figure 18: Examples of traction separation laws for a constant compressive stresses

DISTRIBUTION

1	MS9042	M. Chiesa	8259 (electronic copy)
1	MS9035	P. Spence	8250 (electronic copy)
1	MS9042	A. Brown	8259 (electronic copy)
1	MS9042	S. Nelson	8259 (electronic copy)
1	MS9042	M. Veilleux	8259 (electronic copy)
1	MS9042	J. Dike	8259 (electronic copy)
1	MS9042	N. Spencer	8259 (electronic copy)
1	MS9106	T. Briggs	8226 (electronic copy)
1	MS9042	J. Foulk	8256 (electronic copy)
1	MS0845	J. Jung	1542 (electronic copy)
1	MS0845	K. Pierson	1542 (electronic copy)
1	MS0812	W. Scherzinger	1524 (electronic copy)
1	MS0899	Technical Library	9536 (electronic copy)


Sandia National Laboratories